The 1126 Ma volcanic event in the Dechang Area, SW Yangtze Block and its significance

Chenming Lu[a,b], Chuanheng Zhang[c], Heng Zhang[b,*], Ying Zhou[d], Graham A. Shields[d], Linzhi Gao[b], Xiaozhong Ding[b]

[a]Institute of Hydrogeology and Environmental Geology, Chinese Academy of Geological Sciences, Shijiazhuang 050000, China

[b]Institute of Geology, Chinese Academy of Geological Sciences, Beijing 100037, China

[c]China University of Geosciences, Beijing 100083,China

[d]Department of Earth Sciences, University College London, Gower Street, London, WC1E 6BT, UK

CML, 0000-0002-1231-6294; HZ,

*Correspondence: heng0520@126.com

Abstract

Traditionally, strata of the Luonie Valley, Dechang County, SW Sichuan are considered to contain a suite of felsic volcanic rocks (the Huili Group) that erupted after circa 1050 Ma. However, we report here new age constraints, elemental and Lu-Hf isotope geochemistry for a different suite of older basaltic agglomerate lava, basaltic tuff lava and basalt from the same area, which we name the Luonie Formation. New dating results show that the basaltic volcanic suite of the upper part of the Luonie Formation formed at 1126.1 ±9.9 Ma, significantly earlier than deposition of the Huili Group, but comparable in age to the 1142 ±16 Ma Laowushan Formation in central Yunnan Province. Granite intrusion into the Luonie Formation at 1050.7 ±12.7 Ma provides crucial supporting evidence for this earlier depositional age. We also report a maximum sedimentary age of ca. 1158 Ma for the underlying arkose, implying stratigraphic conformity with the basaltic volcanic rock suite. The Lu-Hf isotope and trace element signatures indicate a depleted mantle source, consistent with a convergent tectonic margin association for the erupted basalts. Lithofacies analysis shows that the basalts extruded onto a littoral-neritic environment, while the underlying arkose exhibits soft-sediment deformation structures that we attribute to

seismic activity. We show here how evidence is consistent with a phase of continental extension that preceded the convergence of the SW Yangtze Block to form part of Rodinia.

Keywords

SW Sichuan; Huili Group; Luonie Formation; Basaltic volcanic rocks; Destructive plate margin tectonic context

Introduction

The tectonic evolution of the ancient Kangtien shield in SW China and its relationship with the supercontinent cycle are still the subject of considerable controversy despite having been the target of several previous studies (Li Z X et al, 2002; Greentree M R et al, 2006; Zhang C H et al, 2007; Geng Y S et al, 2007, 2017; Li H K et al, 2013; Zhou M F et al, 2014; Wang W et al, 2014; Cawood P A et al, 2018; Zhang H et al, 2018). To date, important progress has been made that allows geological events to be divided into three distinct phases: (1) A ~1800 to ~1600 Ma continental rift stage. After the Columbia supercontinent was pieced together around 1800 Ma, a near-east-west continental rift valley was formed, evidenced by the lower portions of the Dahongshan Group (Laochanghe Fm, Manganghe Fm and Hongshan Fm), Hekou Group, Dongchuan Group (Yinmin Fm) and Tongan Formation (First Section) (Greentree M R et al, 2008; Zhao X F et al, 2010, 2011; Yin F G et al, 2012; Yang H et al, 2012; Li H K et al, 2013; Wang D B et al, 2013; Chen W T et al, 2013; Wang W et al, 2014; Ren G M et al, 2014; Pang W H et al, 2015; Wang S W et al, 2016; Geng Y S et al, 2017); (2) A ~1600 to ≤1500 Ma passive margin stage. During this stage, the continental rift was further extended, and the southwestern part of the Yangtze Block developed into a passive continental margin, mainly consisting of upper portions of the the Dahongshan Group (Feiweihe Fm and Potou Fm), Dongchuan Group (Luoxue Fm, Heishan Fm and Lvzhijiang Fm), and Tongan Formation (Second, Third and Fourth Sections) (Yin F G et al, 2012; Li H K et al,

2013; Wang W et al, 2014; Pang W H et al, 2015; Geng Y S et al, 2017); (3) A ~1050 to ~1000 Ma active margin stage. At this time the southwestern margin of the Yangtze Block transformed into an active continental margin, of which the representative stratigraphic units are mainly the Kunyang and Huili groups that formed alongside magmatic arc volcanism (Li Z X et al, 2002; Zhang C H et al, 2007; Geng Y S et al, 2007; Yin F G., 2011, 2012; Li H K et al, 2013; Zhu W G et al, 2016).

Although important progress has been made in the study of this area, controversies persist. The Kunyang Group is generally regarded as the product of later tectonic events that occurred during the amalgamation of Rodinia (Zhang C H et al, 2007; Li H K et al, 2013). Greentree M R et al. (2006) maintained that the oceanic crust of the SW Yangtze Block had subducted before 1142 Ma, and that the Kunyang Group formed in the foreland basin of the orogenic belt (Greentree M R et al, 2006; Li H K et al, 2013). However, Zhang C H et al. (2007) observed that the Kunyang Group exhibits characteristics of a magmatic arc setting, and so is expected to have formed alongside active subduction of oceanic lithosphere no later than basin closure at circa 1142 Ma. Although the convergence of the SW Yangtze Block is controversial, and the mode and mechanism of subduction initiation even less clear, the basaltic volcanic rocks of this study are potentially of great significance due to their association with an active tectonic margin during formation of Rodinia. In this study we …..

Geological setting and rock series

The ancient Kangtien shield is located in SW China and comprises a thick succession of stratigraphic units of Proterozoic age that outcrop discontinuously in a N-S direction and are distributed throughout the Kangding - Dukou - Yuanmou - Yimen area of Yunnan Province. The stratigraphic units of the Kangtien shield in central Yunnan and neighbouring southern Sichuan provinces include the Dahongshan Group, Hekou Group, Dongchuan Group, Tongan Formation, Kunyang Group, Huili Group and Laowushan Formation (Yin F G et al, 2011). The structural geology of the

area is complex with numerous N-S fault zones. The study area is located in the north of the ancient Kangtien shield where the Huili Group comprises the Tianbaoshan, Fengshanying and Limahe formations (Fig. 1). The main studied section is located in Luonie Valley, Dechang County, SW Sichuan, where the traditional Tianbaoshan Formation outcrops.

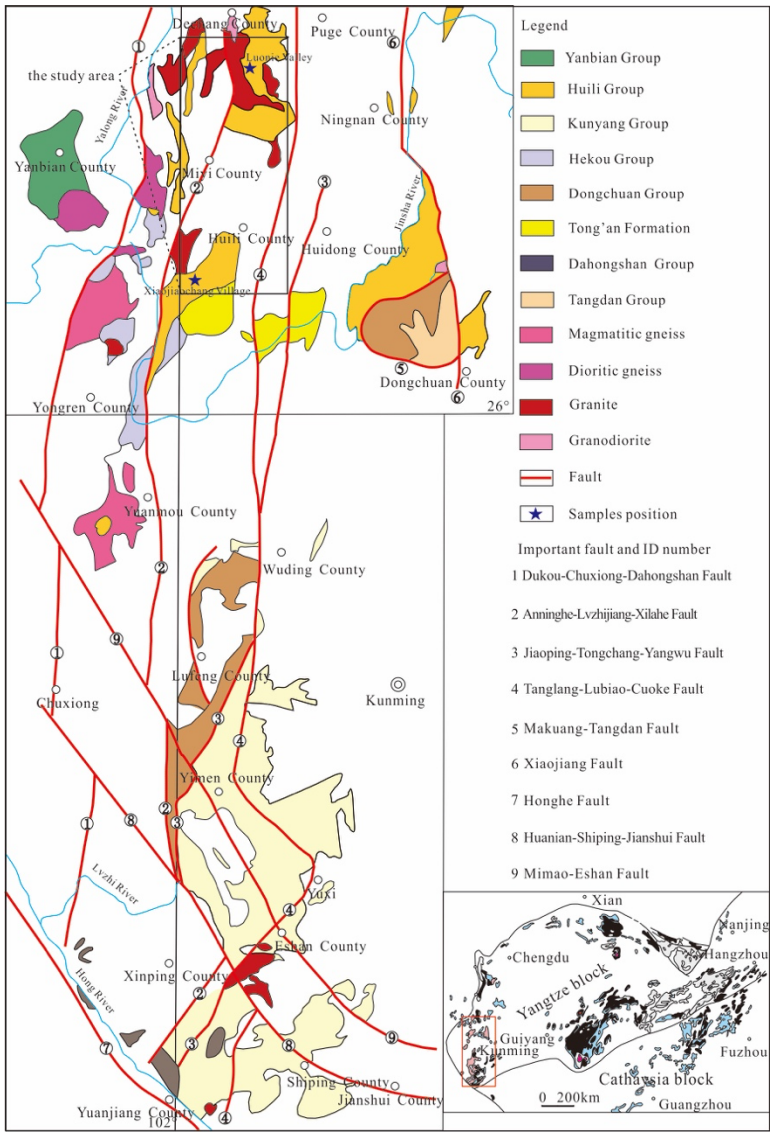

Fig.1. Regional geological map of the SW Yangtze Block showing the distribution of Precambrian strata, plutons and position of the study area

The typical rock types of the Tianbaoshan Formation comprise gray-green sericitic phyllite, metamorphic rhyolitic porphyry, rhyolitic lava and tuff, intercalated with metamorphic sandstone and schist. However, a rock assemblage consisting mainly of volcanic breccia-agglomerate and basic volcanic lava in the Wangxiang Platform, Qipan Mountain and Luonie Valley of west Anning River (Wu G Y, 1986)

was attributed to the Tianbaoshan Formation on the 1:200000 geological map (1996), despite the apparent difference in lithology from the traditional Tianbaoshan Formation. Two rock systems are developed along the Luonie Valley, whereby the lower part is a sedimentary rock series and the upper part a volcanic rock series (Fig. 2), accompanied by intrusive granite (Fig. 4d). The granite intrudes into two rock systems along the weak zone. In addition, the appearance of the two rock systems is parallel, and its contact surface also has no obvious signs of disconformity such as a weathering crust (Fig. 2).

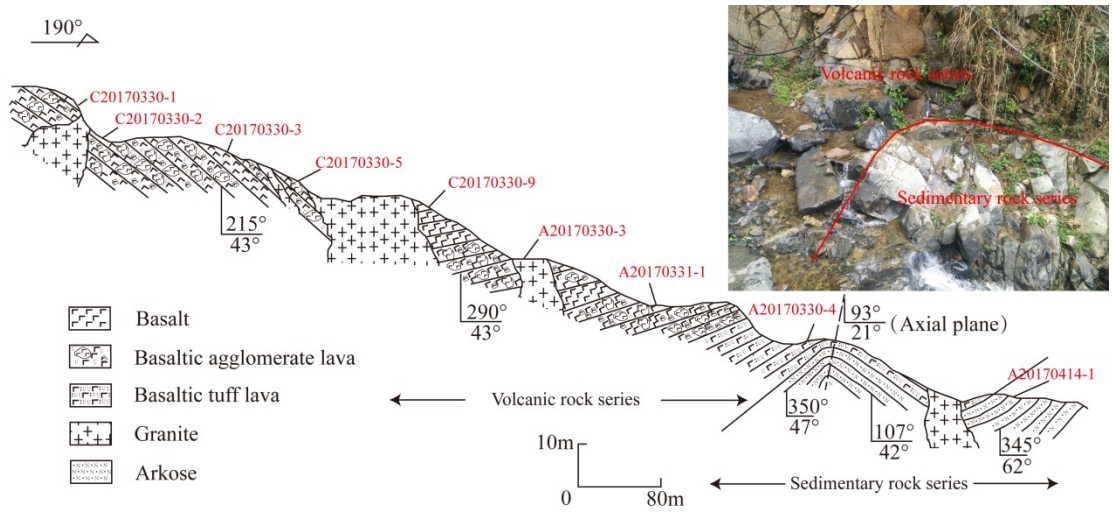

Fig.2. The geological profile of Luonie Valley, locations of samples for zircon U-Pb dating and whole-rock geochemical analyses (A20170330-4, A20170331-1, A20170330-3, A20170414-1, C20170330-1, C20170330-2, C20170330-3, C20170330-5 and C20170330-9)

The sedimentary rock series comprises medium-thick layered arkose (Fig. 3a), mainly composed of feldspar and quartz (Fig. 3b) and a small amount of detrital mica, exhibiting parallel to occasionally oblique bedding as well as abundant evidence for soft-sediment deformation in six distinct forms: 1) Mud flame structures (Fig. 3c) correspond to where the upward movement of argillaceous material has deformed overlying sandstone layers, which retain a smooth and regular cross-section indicative of material flow rather than tectonic deformation. 2) Soft shear slip deformation (Fig. 3d) refers to where sandstone layers comprise imbricated blocks, while the argillaceous rock has remained homogeneous. The different deformation characteristics between these two contrasting lithologies imply that the argillaceous material was not consolidated during deformation. 3) In sliding folds (Fig. 3e), the

sandstone is folded, while the underlying argillaceous rock has not been affected by the deformation. 4) In "S" type flow deformation (Fig. 3f) the surrounding strata are parallel bedding, whereas the "S" deformation has independent deformation characteristics. 5) Sheath folds (Fig. 3g) are arranged between horizontal upper and lower layers. 6) Finally, liquefied veins (Fig. 3h) also occur that cut through overlying strata in wedges and spines, and the whole rock exhibits strong disturbance.

Fig.3. The field photographs and micrograph of the arkose in Luonie Valley: (a) Parallel bedding and oblique bedding of the arkose; (b) Arkose consists mainly of quartz and feldspar. Cross-polarized light; (c) Mud flame structure of the arkose; (d) Soft shear slip deformation of the arkose; (e) Sliding fold of the arkose; (f) "S" type flow deformation of the arkose; (g) Sheath fold of the arkose; (h) Liquefied vein of the arkose

According to the characteristics of the texture and structure, the volcanic rock series can be divided into basaltic agglomerate lava, basaltic tuff lava and basalt. Basaltic agglomerate lava comprises black and gray thickly layered and blocky lava,

including a large number of volcanic agglomerates with occasional xenoliths (Fig. 4a). The aggregates are oval, long and irregularly shaped, and some of them have "S" type deformation. The diameter of aggregates is between 1mm and 50cm, but mainly within the 1-5cm range. On the basis of the crystallization degree and mineral composition of aggregates, they can be divided into agglomerate I, agglomerate II, agglomerate III and agglomerate IV (Fig. 4a, Fig. 4b, Fig. 4e and Fig. 4f); Basaltic tuff lava consists of dark grey thickly layered blocks with cryptocrystalline structure (Fig. 4c); Basalt consists of black and gray thickly layered blocks with cryptocrystalline texture, developing occasionally stomata and almond structure .

In addition, the studied units also include the Limahe Formation of the Huili Group in Xiaojiaochang Village, Huili County (Fig. 1) where the lithology is metamorphic ignimbrite (Fig. 4g). The rock has cryptocrystalline texture and is strongly weathered (Fig. 4h).

Fig.4. The field photographs and micrographs of volcanic rocks in Luonie Valley and ignimbrite in Xiaojiaochang Village: (a) AgglomerateI, agglomerateII, agglomerateIII and xenolith of basaltic agglomerate lava; (b) AgglomerateIV of basaltic agglomerate lava; (c) Basaltic tuff lava; (d) Granite intruded into the basaltic rocks; (e) The contact boundary of the AgglomerateI. Plane-polarized light; (f) The spherical distribution of agglomerateIV. Plane-polarized light; (g) ignimbrite of the Limahe Formation; (g) tuffaceous texture of the ignimbrite

Sample selection and methodology

In this study, five samples for dating (A20170330-4, A20170331-1, A20170330-3, A20170401-1, A20170414-1) and five samples for geochemistry (C20170330-1, C20170330-2, C20170330-3, C20170330-5 and C20170330-9) were collected in Luonie Valley. The samples A20170414-1 and A20170330-3 were collected from the lower sedimentary rock series and the granite, respectively, while the others were taken from the volcanic rock series. In addition, sample A20170401-1 was taken from the top of the Limahe Formation in Xiaojiaochang Village, Huili County (N26°28′35.46″, E102°5′33.15″ (Fig. 1).

Zircon dating of A20170330-4, A20170331-1, A20170330-3 and A20170401-1 was carried out using the SHRIMP II instrument at the Beijing SHRIMP Center, Chinese Academy of Geological Sciences (CAGS). The analytical process was described in detail previously (Lance P B et al, 2003a, 2003b). At the time of testing, the mass resolution of the instrument was about 5000 (1% peak height), and the O^{2-} strength of the primary ion current was between 4~6nA. The diameter of the primary ion current was 25~30 μm, and each data point is made up of 5 scans. Standard zircon TEM and M257 were used for fractionation correction and U content calibration. The processing of the original data and the drawing of the zircon $^{206}Pb/^{238}U$ concordia plot were conducted using the Squid and Isoplot programs written by Dr. Ludwig (Ludwig K R, 2002). The correction for common Pb is deduced from the measured Pb, and the model of Stacey J S (1975), which estimates the isotopic composition of common Pb. In the table, 1σ of the age error is an absolute error, and 1σ of the isotope ratio error is a relative error. The weighted average zircon $^{206}Pb/^{238}U$ age has a 95% confidence coefficient.

Zircon dating of A20170414-1 was carried out using LA-ICP-MS at the Wuhan Sample Solution Analytical Technology Co. In the analysis, the excimer laser GeoLasHd was used for denudation sampling, and the Agilent 7900 four-stage rod plasma mass spectrometer was used to test the ion signal strength. The relevant parameters are laser energy 80 mJ, frequency 5 Hz, laser beam spot diameter 32 m. The specific analytical conditions and procedures are detailed in the literature (Liu Y S et al., 2008, 2010).

Zircon Lu-Hf isotope compositions of the dated zircon grains were analyzed using a Geolas 193 nm excimer ArF laser-ablation system, attached to a Nu Plasma MC–ICP–MS, at Northwest University, Xi'an, China. A stationary spot was used with a beam diameter of 44μm, a 5Hz repetition rate and a laser power of 6J/cm^2. Fractionation correction of the Lu-Hf isotope ratios was calculated using index law, and $^{176}Lu/^{175}Lu$=0.02656 and $^{176}Yb/^{173}Yb$=0.78696 were used to deduce the influence of ^{176}Lu and ^{176}Yb on ^{176}Hf. The ratio of Hf isotopes to Lu isotopes was corrected using $^{179}Hf/^{177}Hf$=0.7325, while the Yb isotope ratios were corrected using $^{173}Yb/^{171}Yb$=1.12346. International standard zircons 91500 and Mudtank were used as reference standards.

The geochemical tests were carried out by the laboratory of regional geology and mineral survey research institute, Hebei Province. Samples were crushed and powered to at least 200 mesh in an agate mill. Major elements were determined by ICP-HEX-MS, the accuracy of which is ±1%. Trace and rare earth elements were determined using plasma mass spectrometry (Element 2) and X-ray fluorescence spectrometry with analytical uncertainties between 1% and 5%.

Results

Geochronological results

Under the microscope, the zircons present as stubby crystals with an aspect ratio of about 2:3. In addition, the zircons have typical oscillatory zones and rhythmic structure, which tends to confirm their magmatic origin (Fig. 5). For the selection of

zircon grains and dating microzones, the authors selected zircon grains that were not too bright or too dark by combining transmission light, reflected light and CL images, and avoided inclusions and cracks in the zircon crystals. The selected microzones for dating were located in obviously magmatic oscillatory zones.

Sample A20170330-4 is basaltic tuff lava. A total of 18 data points were obtained for this sample (Table. 1). 6 data points were removed due to their higher ^{204}Pb and discordant. The projection ellipse of the remaining 12 points lies on or close to the concordia line in the U-Pb concordia plot. The weighted average $^{206}Pb/^{238}U$ age is 1126.1 ±9.9 Ma (MSWD 0.26) (Fig. 6a).

Fig.5. Cathodoluminescence images of analyzed zircons from sample A20170330-4, A20170331-1, A20170401-1 and A20170330-3

Sample A20170331-1 is basalt. In total, 15 data points were obtained for the sample (Table. 1). Five points were eliminated due to their higher U and higher ^{204}Pb, which are 1031 Ma, 1032 Ma, 1052 Ma, 1056Ma and 1615 Ma. The other datas of sample A20170331-1 are all greater than 1070 Ma. The weighted averaged $^{206}Pb/^{238}U$

age is 1100.1 ±11.2 Ma (MSWD 1.49) (Fig. 6b).

Sample A20170330-3 is granite. In total, 15 data points were obtained for the sample (Table 1), one of which were eliminated due to its higher U. The weighted averaged $^{206}Pb/^{238}U$ age is 1050.7 ±12.7 Ma (MSWD 1.74) (Fig. 7a)..

Sample A20170401-1 is an ignimbrite. A total of 12 data points were obtained for this sample (Table 1). However, 6 data points were eliminated because of high U, high Th/U, high ^{204}Pb and discordant. The weighted average $^{206}Pb/^{238}U$ age is 1033.1±14.8 Ma (MSWD 1.48) (Fig. 7b).

Sample A20170414-1 is an arkose. A total of 54 data points were obtained for this sample (Table. 2). The confidence of all data is greater than 90%. Two maximum ages were obtained for this sample, which are respectively 1158 ±9 Ma and 1183 ±9 Ma (Fig. 8).

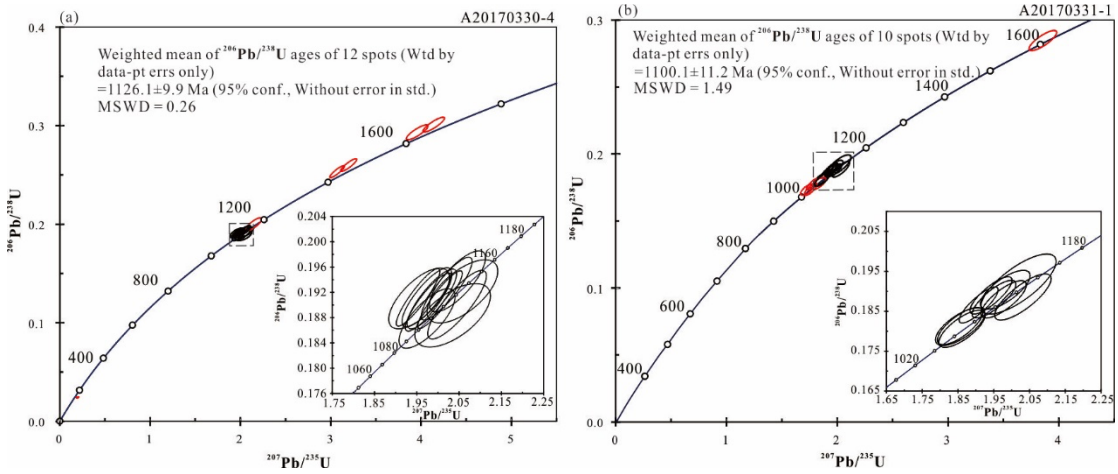

Fig.6. SHRIMP zircon U-Pb concordia plots from A20170330-4 (Basaltic tuff lava) and A20170331-1 (Basalt)

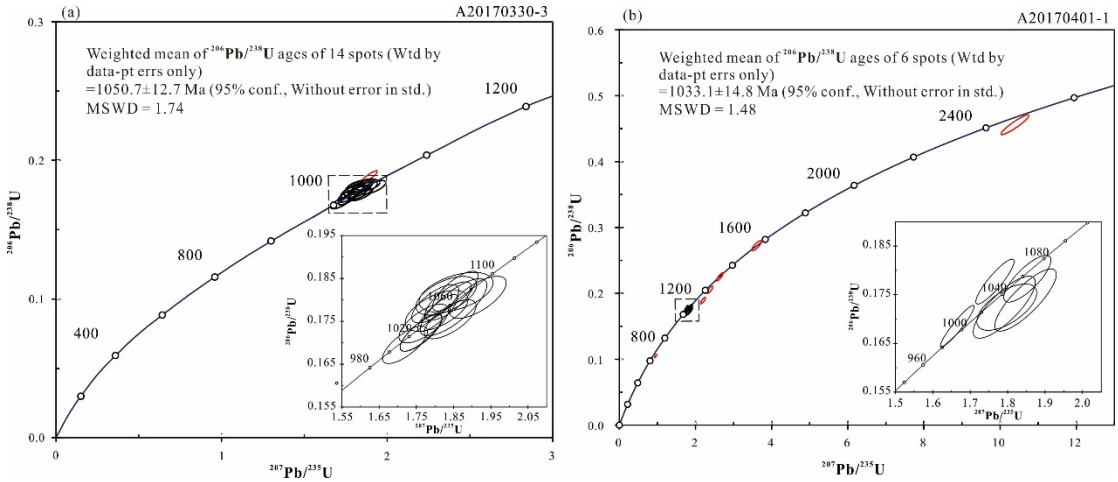

Fig.7. SHRIMP zircon U-Pb concordia plots from A20170330-3 (Granite) and A20170414-1 （Ignimbrite）

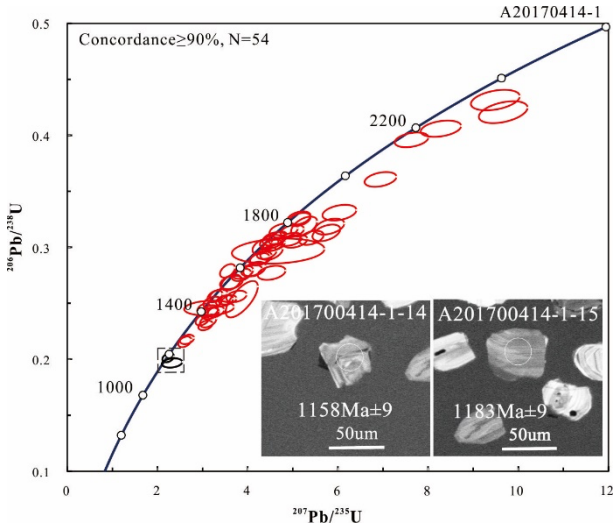

Fig.8. Zircon U-Pb concordia plot of arkose rock from sample A20170414-1

Zircon Lu-Hf isotopes

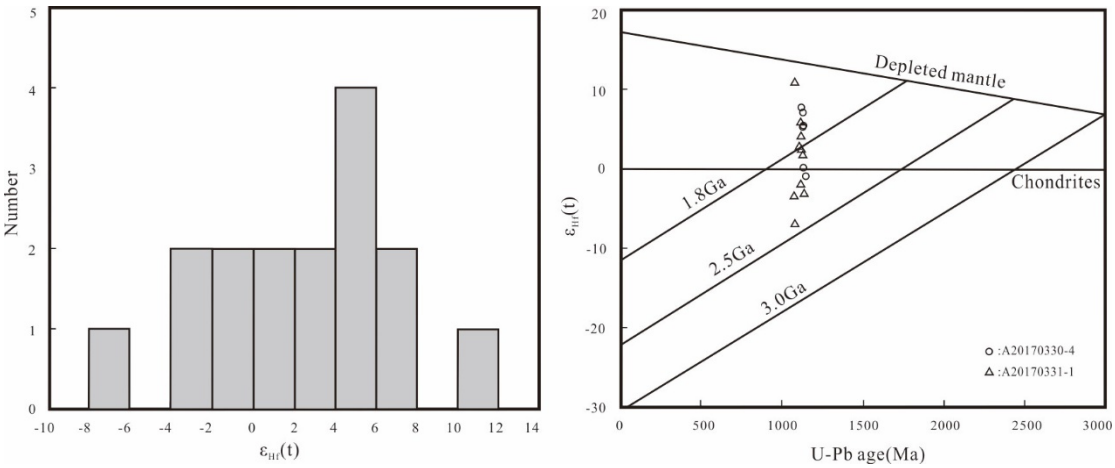

Fig.9. $\varepsilon_{Hf}(t)$ histogram and age -$\varepsilon_{Hf}(t)$ plot of the basaltic volcanic rocks from sample A20170330-4 and A20170331-1

The Lu-Hf isotope compositions of the zircons were analyzed in the same microzone position as that used for zircon U-Pb dating. Before Lu-Hf isotope data analysis, the authors first removed the data from samples exhibiting higher U and higher error correlation coefficients, i.e. for samples A20170330-4 and A20170331-1, from the U-Pb dating. In addition, the data with $^{176}Lu/^{177}Hf$ ratios greater than 0.002 were also eliminated because only when the $^{176}Lu/^{177}Hf$ ratio is less than 0.002 can the $^{176}Lu/^{177}Hf$ ratio represent the Hf isotope composition of the source region (Wu Y

F et al, 2007). The remaining 16 data points were used for data analysis (Table 3). Because samples A20170330-4 and A20170331-1 are both basaltic volcanic rocks from the same horizon, they are considered and displayed together. $\varepsilon_{Hf}(t)$ values of all the data points lie in the range -6.9 to +10.9, with a weighted mean of 2.4, and so the data set sits mainly above the Hf isotope evolution line of chondrites (Fig. 9). The single-stage Hf model age of the 16 data points range between 1320 Ma and 1869 Ma, with a weighted mean of 1536 Ma. The two-stage Hf model age ranges between 1222 Ma and 2359 Ma, with a weighted mean of 1799 Ma.

Geochemical results

The SiO_2 content of volcanic rock samples is 46.42% - 48.47%, the K_2O content is 0.5% - 0.75%, and the Na_2O content is 2.01% - 3.12%, all of which confirm that they are of basaltic composition (Fig. 10).

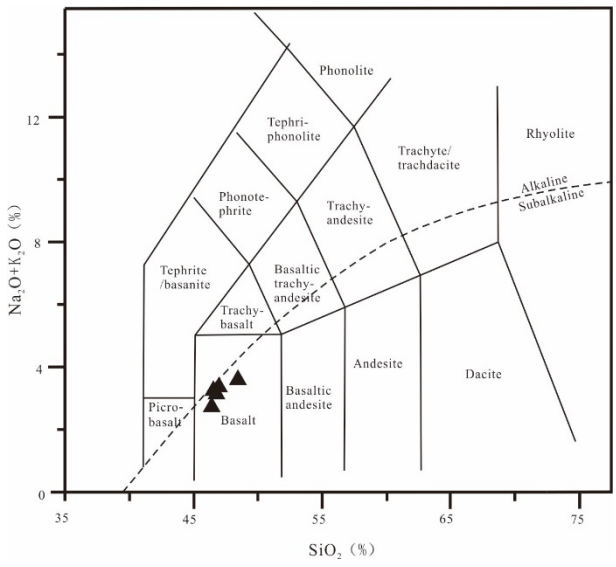

Fig.10. TAS classification diagram of the volcanic rocks in Luonie Valley

In general, the light rare earth elements (LREE), K_2O and Na_2O are enriched in crustal components, while P_2O_5, TiO_2, CaO and MgO tend to be deficient. Conversely, mantle-derived components show reversed characteristics (Sun S S et al, 1989; Wang D B et al, 2013). In this study, the LREE of the basaltic volcanic rocks are slightly enriched relative to the HREE with LREE/HREE = 2.98-3.88 and $(La/Yb)_N$ =3.21-4.59 (Table. 4; Fig. 11a). Other large ionic lithophile elements (Rb, Ba, Th, U,

K) are also enriched relative to the mantle (Sun S S et al, 1989). Furthermore, Pb showed a positive anomaly, while P showed a slight negative anomaly (Fig. 11b).

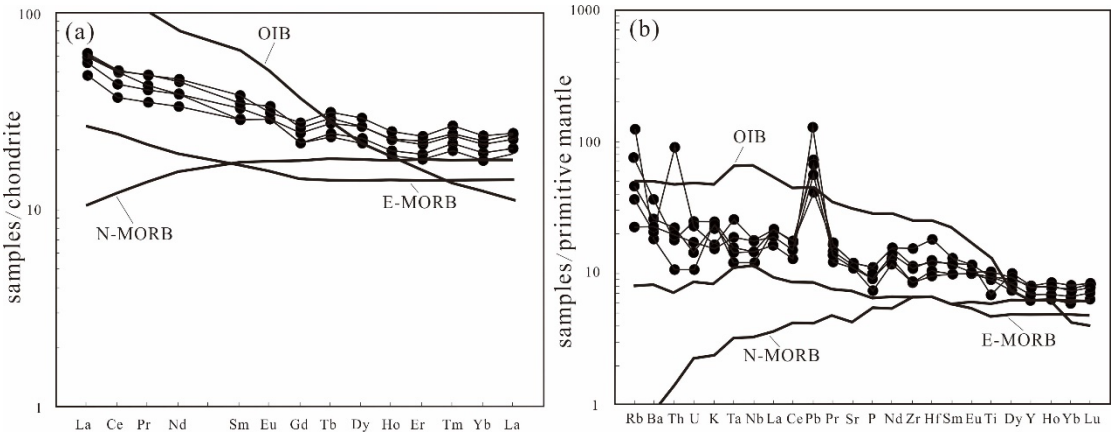

Fig.11. Distribution pattern diagrams of the volcanic rocks in Luonie Valley: (a) Rare earth elements; (b) Trace elements (chondrite and primitive mantle from McDonough W F et al (1995); the values of OIB, E-MORB and N-MORB from Sun S S et al (1989));
OIB：Oceanic island basalt; E-MORB: exceptional mid-ocean ridge basalt; N-MORB：normal mid-ocean ridge basalt.

Discussion

Soft-sediment deformation structures

There are many ways to cause soft-sediment deformation besides earthquakes, e.g. rapid accumulation, flowing water, wave action and tsunami. For many years, scholars have been studying the distinguishing marks of soft-sediment deformation structures caused by earthquakes (Berra F et al, 2011; Moretti M et al, 2007; Ettensohn F R et al, 2002; Montenat C et al, 2007; Du Y S et al, 2000; Obermeier S F et al, 1996), whereby liquefied veins are generally regarded as one of the important criteria to recognize seismites (Plaziat et al, 1990; Liang D Y et al, 1994; Obermeier S F et al, 1996; Rodriguez-Pascua et al, 2000; Qiao X F et al, 2002; Zhang C H et al, 2006). In the Luonie Valley arkose, there are many soft-sediment deformation structures (examples see Fig. 3c-h), including liquefied veins, which supports the hypothesis that the soft-sediment deformation was caused by frequent seismic activity, consistent with the transition from an active tectonic to an eruptive volcanic setting.

Volcanic lithofacies

Volcanic lithofacies can be divided into continental and marine facies (Xu X S et al, 2010). The volcanic rocks of continental facies are usually reddish or purplish brown in color. Meanwhile, the weathering crust is more developed, and the contact relationship with the underlying strata is generally unconformable. Pyroclastic materials also account for a large proportion of the rock composition, and the sorting of fragments is poor. The composition of continental lava ranges from mafic to felsic, often developing columnar joints. By contrast, marine volcanic rocks generally exhibit the opposite features. The basaltic volcanic rocks of Luonie Valley are dark-grey to grey-black, and their lithology is relatively homogeneous. Furthermore, there is an apparently transitional and thus conformable contact relationship with the underlying arkose, and no weathering crust has been formed. In summary, it shows the characteristics of marine volcanic rocks. However, the basaltic volcanic rocks also simultaneously have some important characteristics of continental volcanic rocks, such as a relatively high proportion of pyroclasts, poor sorting of aggregates and no pillow structure. Therefore, the basaltic volcanic rocks most likely formed in a littoral-neritic environment quite different from N-type MORB.

Age of the Luonie Formation

In this study, zircons from the ignimbrite at the top of the Limahe Formation were dated at 1033.1±14.8 Ma. Although the age and other published ages do not represent the base of the Huili Group (Zhang C H et al, 2007; Geng Y S et al, 2007; Li H K et al, 2013), the age of the base is not expected to be significantly different. The new dated ages in this study for the basaltic rocks of Luonie Valley of 1126.1±9.9 Ma and 1100.1 ±11.2 Ma are much older than published ages of the Huili Group, indicating that there was an important volcanic event before deposition of the Huili Group in the Dechang area of SW Sichuan. Although some younger points were removed from the 1100.1 ±11.2 Ma, this was due to their anomalously high U, high ^{204}Pb. All other determined ages are greater than 1070 Ma.

Before discussing the significance of these basalt ages, the presence of

comagmatic zircons in presumably silica unsaturated basalt may be questioned. The melt system and the fluid system can be seen as two independent geological systems according to transmagmatic fluid metallogenesis theory (Fuentes M, 1965; Luo Z H et al, 2007). Magma can also be viewed as a mixture of melt, fluid, and even solid (Burgisser A et al, 2005; Bachmann O et al, 2008; Miller C F et al, 2008). Because zirconium tends to concentrate in the fluid phase during partial melting and crystallization, the concentration of Zr in fluids can increase by 2-3 orders of magnitude, especially if the fluid system contains $NaHCO_3$ (Pouchon M A et al, 2001). The crystallization of biotite in basalt can consume magma volatiles, reducing the solubility of Zr and leading to zircon crystallization (Luo Z H et al, 2006). As a consequence, zircons are commonly found not only in basic rocks, but also in ultrabasic rocks (Yu S C et al, 2001).

Our argument, however, does not rest solely on the determined U-Pb ages of the extrusive basalts. Granite intrusion into these basaltic rocks at 1050.7 ±12.7 Ma provides key supporting evidence that the basaltic rocks do not belong to the Tianbaoshan Formation, and the age is about 50Ma younger than 1100.1 ±11.2 Ma of the basalt age. The maximum sedimentary age of the arkose at ca. 1158 Ma also implies likely continuity between the underlying sedimentary rock series and the overlying volcanic rock series. The observation that detrital zircon age peaks are different for the Huili Group than the Kunyang Group supports this still further.

Comparably, tuff from the Laowushan Formation underlying the Kunyang Group yielded an age of 1142 ±16 Ma in the Yimen area of central Yunnan, which is the only previous evidence for a stratigraphic unit of about 1150 Ma in the coeval Kangtien succession (Greentree M R et al, 2006) (Fig. 12). However, the Laowushan Formation and the basaltic volcanic rocks described here are exposed in different areas, and so may be the products of contemporaneous but different settings. With the new age, the sedimentary rock series and volcanic rock series in Luonie Valley can be correlated to the Laowushan Fm in central Yunnan. Therefore, the present authors suggest that these two units should be separated from overlying Huili Group, and collectively be renamed the Luonie Formation.

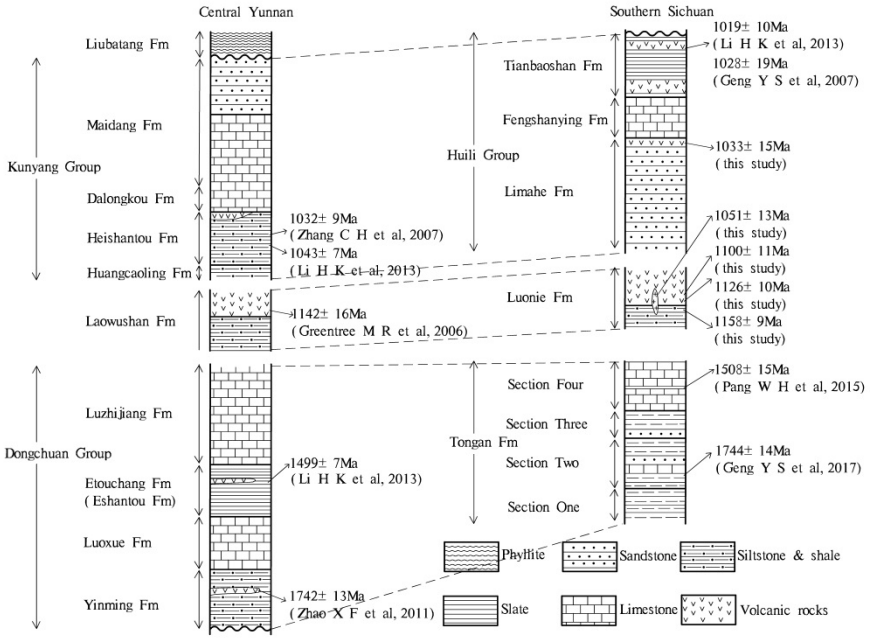

Fig.12. Comparison and correlation of the different stratigraphic systems used for the late Paleo - Mesoproterozoic in Central Yunnan and Southern Sichuan

Tectonic environmental analysis

Zircon Lu-Hf isotope data show that the $\varepsilon_{Hf}(t)$ values of the basaltic volcanic rocks are mostly positive. Although the single-stage Hf model ages and the two-stage Hf model ages are different from the formation age, this only indicates that it is slightly miscible with crustal materials. Therefore, the magmatic source of the basaltic volcanic rocks likely still originated from the depleted mantle, which further shows that it had formed under the upwelling mantle material within an extensional regime.

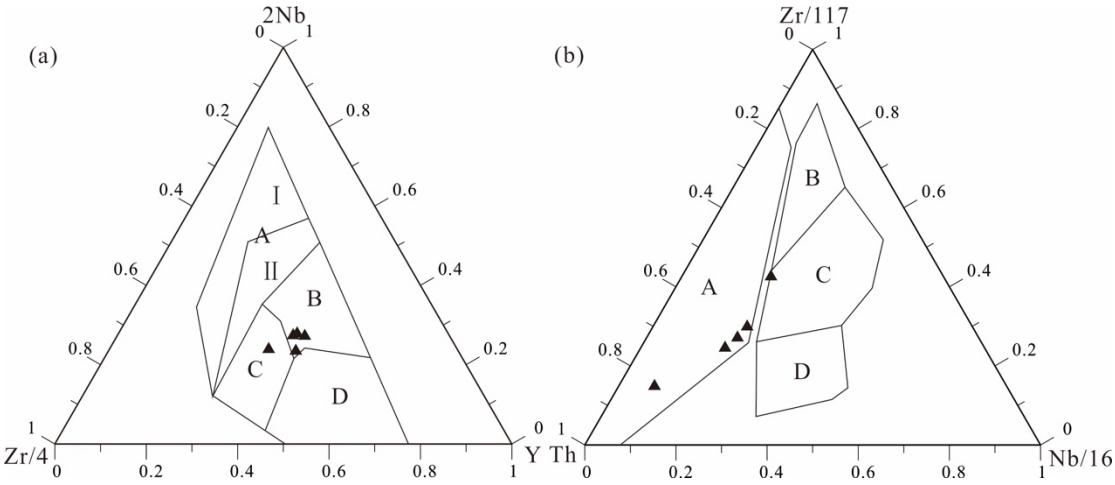

Fig.13. Trace elements discrimination diagram of the volcanic rocks in Luonie Valley (Meschede

M et al, 1986; Wood D A et al, 1979): (a) AⅠ: Alkaline basalt of intraplate; AⅡ: Alkaline basalt and tholeiite of intraplate; B: E-type MORB; C: Tholeiite of intraplate and volcanic arc basalt; D: N-type MORB and volcanic arc basalt; (b) A: Basalt of the destructive plate margin; B: N-type MORB; C: E-type MORB; D: Basalt of intraplate

According to the trace element analysis, the REE distribution pattern shows a slight enrichment of LREE, while the HREE are relatively deficient. The distribution pattern is therefore similar to E-type MORB. Likewise, the trace element spider diagram shows enrichment in large ionic lithophile elements, with the exception of Y, Ho, Yb and Lu. In summary, the trace element distribution is also similar to E-type MORB with the exception Pb and P anomalies. In order to further determine the tectonic setting of the basaltic volcanic rocks, we applied the triangular discrimination diagrams Zr/4-Y-2Nb and Th-Nb/16-Zr/117. The data points mainly fall into the area of E-type MORB in the Zr/4-Y-2Nb discrimination diagram (Fig. 13a), which is consistent with the conclusion of trace metal analysis. Further, the Th-Nb/16-Zr/117 discriminating diagram distinguishes destructive plate margin basalt from the E-type MORB, and the data points mainly fall in the former region (Fig. 13b). Therefore, the basaltic volcanic rocks of the Luonie Formation should have formed in a destructive plate margin tectonic context.

Evolution process

Through the analysis of sedimentary facies and geochemical data, there is reliable evidence for a continental shelf and continental slope of a passive continental margin on the SW Yangtze Block before 1500 Ma (Yin F G et al, 2012; Li H K et al, 2013; Wang W et al, 2014; Pang W H et al, 2015; Geng Y S et al, 2017). At present, exactly when this tectonic setting changed is not clear. In addition, the lithology and geochemical characteristics of the Kunyang and Huili groups indicate that they should have formed at an active continental margin, but consensus regarding the convergence time of the SW Yangtze Block has not been reached (Li Z X et al, 2002; Zhang C H et al, 2007; Geng Y S et al, 2007; Yin F G., 2011, 2012; Li H K et al, 2013; Zhu W G et al, 2016). The 1126.1±9.9 Ma age of basaltic volcanic rocks and the 1142 ±16 Ma age of the Laowushan Formation need to be taken into account. Greentree M R et al.

(2006) maintained that the Laowu Formation was formed after the Sibao Orogeny. However, evidence from this study indicates a different tectonic evolution before and after the 1150 Ma.

According to the above analysis, two tectonic evolutionary stages emerge represented by the sedimentary arkose and the basaltic volcanic rocks, respectively. Firstly, the arkose represents the active stage in the development of a passive continental margin. At this stage, the upwelling of mantle magma enhanced the tectonic uplift and seismic activity leading to the formation of soft-sediment deformational structures (Fig. 14a). Starting from 1126.1±9.9 Ma, the tectonic context completely changed. The passive continental margin began to rift apart, causing eruption of the basaltic volcanic rocks of E-type MORB in the littoral-neritic environment (Fig. 14b). The passive continental margin then developed into an active continental margin, after which island arc-type volcanic rocks of the Tianbaoshan Formation (Huili Group) were formed. The transition may have occurred earlier than 1033 Ma (Fig. 14c). The basaltic volcanic rocks of the Luonie Formation erupted during an important interval between rupture of the supercontinent Columbia and convergence of Rodinia. They should represent the onset and transition mechanism of the convergence of the SW Yangtze Block.

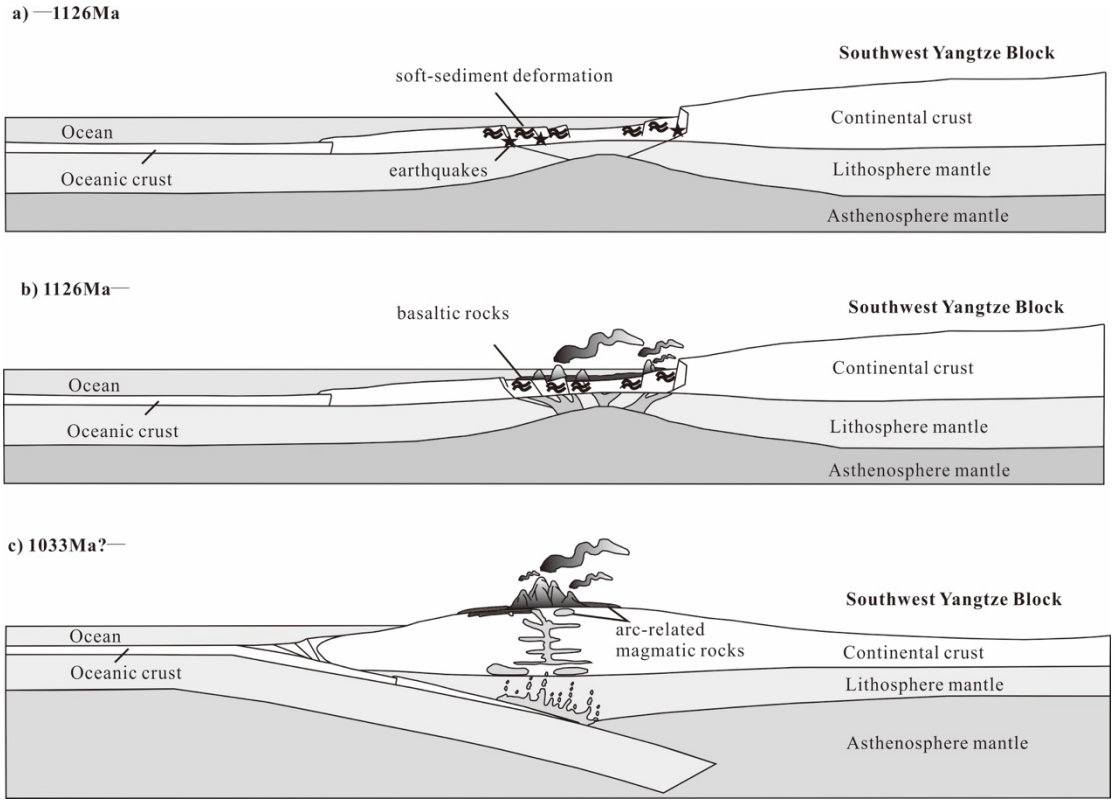

Fig.14. Development of the tectonic setting during the late Mesoproterozoic in Dechang area, SW Yangtze Block: (a) The upwelling of mantle magma enhanced the tectonic uplift and seismicity activity; (b) The rift caused the eruption of basaltic volcanic rocks; (c) The active margin of the Huili Group

Conclusions

1. Basaltic volcanic rocks erupted in a littoral-neritic environment around 1126.1±9.9 Ma and an underlying sedimentary arkose unit was formed no earlier than ca. 1158±9 Ma, respectively. Here we rename these two units together as the Luonie Formation.

2. Soft-sediment deformation structures within the arkose were likely caused by seismic activity, indicating that major earthquakes were common during this period. However, the transition to basaltic volcanic rocks implies a subsequent change in tectonic setting.

3. Lu-Hf isotopes indicate that the magmatic source of the basaltic volcanic rocks was the depleted mantle, following upwelling of mantle material under an extensional regime. Trace element characteristics further confirm that they formed

behind a destructive, convergent plate margin.

4. Two distinct tectonic evolutionary stages can be inferred from deposition of the arkose to eruption of the basaltic volcanic rocks. The arkose represents the active stage of a passive continental margin, while the basaltic volcanic rocks reflect its rifting. The evolution represents the onset and transition to convergence of the SW Yangtze Block.

Acknowledgments

Biao Song of Beijing SHRIMP Center, Zhian Bao of the Continental dynamics laboratory, Northwest University, and other workers are greatly appreciated for their assistances with the analyses.

Author contributions

CML: conceptualization (lead), formal analysis (lead), investigation (lead), visualization (lead), writing-original draft (lead), writing-review & editing (lead); CHZ: data curation (lead), formal analysis (equal), investigation(equal), writing-review & editing (supporting); HZ: formal analysis(equal), investigation (equal), visualization (supporting), writing-review & editing (supporting); YZ: formal analysis (supporting), writing-review & editing (supporting); GAS: formal analysis (supporting), writing-review & editing (supporting); LZG: conceptualization (supporting), formal analysis (supporting), writing — review & editing (supporting); XZD: data curation (supporting), formal analysis (supporting), writing-review & editing (supporting)

Funding information

This research was supported by the National Natural Science Foundation of China (No.41572024), Geological Tectonic Division and Comprehensive Integration of Regional Survey of China (No.DD20190370), the Fundamental Reasearch Fund for

the Chinese Academy of Geological Sciences (No.JYYWF20181302), Geological Survey Projects Foundation of Institute of Hydrogeology and Environmental Geology (No.DD20190252; No.DD20190303) and Technology Innovation Center of Geothermal & Hot Dry Rock Exploration and Development, Ministry of Natural Resources.

Data availability statements

All data generated or analysed during this study are included in this Published article (and its supplementary information files).

References

Berra F, Felletti F. Syndepositional tectonics recorded by soft-sediment deformation and liquefaction structures continental Lower Permian sediments, Southern Alps, Northern Italy:stratigraphic significance. Sedimentary Geology, 2011, 235: 249~263, DOI: 10.1016/j.sedgeo.2010.08.006

Bachmann O, Bergantz G W. Deciphering magma chamber dynamics from styles of compositional zoning in large silicic ash flow sheets. Reviews in Mineralogy and Oeochemistry, 2008, 69: 651~674, DOI: 10.2138/rmg.2008.69.17

Burgisser A, Bergantz G W, Breidenthal R E. Addressing complexity in laboratory experiments: The scaling of dilute multiphase flows in magmatic systems. Journal of Volcanology and Geotherm al Research, 2005, 141: 245~265, DOI: 10.1016/j.jvolgeores.2004.11.001

Cawood P A, Zhao G C, Yao J L, Wang W, Xu Y J, Wang Y J. Reconstructing South China in Phanerozoic and Precambrian supercontinents. Earth-Science Reviews, 2018, 186: 173–194, DOI: 10.1016/j.earscirev.2017.06.001

Chen W T, Zhou M F, Zhao X F. Late Paleoproterozoic sedimentary and mafic rocks in the Hekou area, SW China: Implication for the reconstruction of the Yangtze Block in Columbia. Precambrian Research, 2013, 231: 61~77, DOI: 10.1016/j.precamres.2013.03.011

Du Y S, Han xin. Seismo-deposition and seismites. Advanced in Earth Sciences. 2000, 15(4):

389~394 (in Chinese with English Abstract), DOI: 10.3321/j.issn:1001-8166.2000.04.005

Ettensohn F R, Rast N, Brett C E. Ancient Seismites. Geological Society of America, Special Paper, 2002, DOI: 10.1029/2003EO140009

Fuentes M . The most important syndromes of the ocular system. IV. Neurological findings of the optical nerve syndrome. Gaceta medica de Mexico, 1965, 95(2):123~127, DOI: 10.1007/BF02764500

Greentree M R, Li Z X, Li X H, et al. Late Mesoproterozoic to earliest Neoproterozoic basin record of the Sibao orogenesis in western South China and relationship to the assembly of Rodinia . Precambrian Research, 2006, 151: 79~100, DOI: 10.1016/j.precamres.2006.08.002

Greentree M R, Li Z X. The oldest known rocks in south-western China:SHRIMP U-Pb magmatic crystallization age and detrital provenance analysis of the Paleoproterozoic Dahongshan Group. J. Asian Earth Sci, 2008, 33: 289~302, DOI: 10.1016/j.jseaes.2008.01.001

Geng Y S, Yang C H, Du L L, Wang X S, Ren L D, Zhou X W. Chronology and Tectonic Environment of the Tianbaoshan Formation :New Evidence from Zircon SHRIMP U-Pb Age and Geochemistry. Geological Review, 2007, 53(4): 556~563(in Chinese with English Abstract), DOI:10.1016/S1872-5791(07)60044-X

Geng Y S, Kuang H W, Liu Y Q, Du L L. Subdivision and correlation of the Mesoproterozoic stratigraphy in the Western and Northern margins of Yangtze block. Acta Geologica Sinica, 2017, 91(10): 2151~2174 (in Chinese with English Abstract), DOI: 10.3969/j.issn.0001-5717.2017.10.001

Lance P B, Sandra L K, Charlotte M A, et al. TEMORA 1: a new zircon standard for Phanerozoic U-Pb geochronology. Chemical Geology, 2003a, 200: 155~170, DOI:10.1016/S0009-2541(03)00165-7

Lance P B, Sandra L K, Ian S Williams, et al. The Application of SHRIMP to Phanerozoic geochronology: a critical appraisal of four zircon standards. Chemical Geology, 2003b, 200: 171~188, DOI: 10.1016/S0009-2541(03)00166-9

Liang D Y, Nie Z T, Song Z M. A Re-study on Seismite and Seismo—Unconformity: Taking Western Sichuan and Western Yunnan as an Example. Earth Science-Journal of China University of Geoscience, 1994, 19(6) : 845~850 (in Chinese with English Abstract).

Li H K, Zhang C L, Yao C Y, Xiang Z Q. Zircon U-pb age and Hf isotope composition of

Mesoproterozoic sedimentary strata on the western margin of the Yangtze massif. Chinese Science: Earth Science, 2013, 43(8): 1287~1298 (in Chinese without English abstract), DOI: 10.1007/s11430-013-4590-9

Li Z X, Li X H, Zhou H, et al. Grenvillian continental collision in South China: new SHRIMP U-Pb zircon results and implications for the configuration of Rodinia. Geology, 2002, 30: 163~166, DOI: 10.1130/0091-7613(2002)0302.0.CO;2

Ludwig K R. SQUID 1.02, a user's manual. Berkeley Geochronology Center Special Publication, USA, 2002.

Liu Y S, Hu Z C, Gao S, Günther D, Xu J, Gao C G, Chen H H. In situ analysis of major and trace elements of anhydrous minerals by LA-ICP-MS without applying an internal standard. Chemical Geology, 2008, 257: 34~43, DOI: 10.1016/j.chemgeo.2008.08.004

Liu Y S, Gao S, Hu Z C, Gao C G, Zong K Q, Wang D B. Continental and oceanic crust recycling-induced melt-peridotite interactions in the Trans-North China Orogen: U-Pb dating, Hf isotopes and trace elements in zircons of mantle xenoliths. Journal of Petrology, 2010, 51: 537~571, DOI: 10.1093/petrology/egp082

Luo Z H, Mo X X, Wan Y S, Li L, Wei Y. Geological implications of the youngest SHRIMP U-Pb age of the alkaline basalt in the Tibetan Plateau. Acta Petrologica Sinica, 2006, 22(3): 578~584 (in Chinese with English abstract), DOI: 10.1016/j.sedgeo.2005.12.020

Luo Z H, Mo X X, Lu X X, Chen B H, Ke S, Hou Z Q, Jiang W. Metallogeny by trans-magmatic fluids-theoretical analysis and field evidence. Earth Science Frontiers, 2007, 14(3): 165~183 (in Chinese with English abstract), DOI: 10.1016/j.sedgeo.2005.12.020

Miller C F, Wark D A. Supervolcanoes and their explosive supereruptions. Elements, 2008, 4: 11~16, DOI: 10.2113/gselements.4.1.11

McDonough W F, Sun S S. The composition of the Earth. Chemical Geology, 1995, 120(3/4): 223~253, DOI: 10.1016/0009-2541(94)00140-4

Meschede M. A method of discriminating between different types mid-ocean ridge basalts and continental tholeiites with the Nb-Zr-Y diagram. Chem Geol, 1986, 56: 207~218, DOI: 10.1016/0009-2541(86)90004-5

Montenat C, Barrier P, Ottd N, et al. Seismites: An attempt at critical analysis and classification. Sedimentary Geology, 2007, 196: 5~30, DOI: 10.1016/j.sedgeo.2006.08.004

Moretti M, Sabato L. Recognition of trigging mechanisms for soft-sediment deformation in the Pleistocene lacustrine depositions of the Sant Arcangelo Basin(Southern Italy): Seismis Shock vs overloading. Sedimentary Geology, 2007, 196: 31~45, DOI: 10.1016/j.sedgeo.2006.05.012

Obermeier S F. Use of liquefaction-induced features for paleoseismic analysis an overview of how seismic liquefaction features can be distinguished from other features and how their regional distribution and properties of source sediment can be used to infer the location and strength of Holocene paleo-earthquakes. Engineering Geology, 1996, 44(1): 1~76, DOI: 10.1016/S0013-7952(96)00040-3

Pouchon M A, Curti E, Degueldre C. The influence of carbonate complexes on the solubility of zirconia: New experimental data. Progress in Nuclear Energy, 2001, 38(3-4): 443~446, DOI: 10.1016/S0149-1970(00)00155-4

Plaziat J C, Purser B H, Philobbos E R. Seismic deformation structures (seismites)in the syn-rift sediments of the NW Red Sea(Egypt). Bulletin de la Société Géologique de France, 1990, 6(3): 419~434, DOI: 10.2113/gssgfbull.VI.3.419

Pang W H, Ren G M, Sun Z M, Yin F G. Division and correlation of Mesoproterozoic strata on the western margin of Yangtze block: Evidence from the U-Pb age of tuff zircon in the Tongan Formation. Geology in China, 2015, 42(4): 921-936 (in Chinese with English abstract).□□

Qiao X F. Intraplate seismic beltand basin framework of sino korean plate in Proterozoic. Earth Science Frontiers, 2002, 9(3): 141~149 (in Chinese with English abstract).

Rodriguez-Pascua M A, Calvo J P, De Vicente G, et al. Soft-sediment deformation structures interpreted as seismites in lacustrine sediments of the Prebetic Zone, SE Spain, and their potential use as indicators of earthquake magnitudes during the Late Miocene. Sedimentary Geology, 2000, 135(1): 117~135, DOI: 10.1016/S0037-0738(00)00067-1

Ren G M, Pang W H, Sun Z M, Yin F G. Zircon U-Pb chronology of the amphibolite of Tongan Formation and its geological significance. Journal of Mineralogy and Petrology, 2014, 34(2): 33-39 (in Chinese with English abstract).

Stacey J S, Kramers J D. Approximation of terrestrial lead isotope evolution by two-stage model. Earth and Planetary Science Letters, 1975, 26: 207~221, DOI:

10.1016/0012-821X(75)90088-6

Sun S S, McDonough W F. Chemical and isotopic systematics of oceanic basalts; implications for mantle composition and processes. Geological Society Special Publications, 1989, 42: 313~345, DOI: 10.1144/GSL.SP.1989.042.01.19

Wood D A. A reappraisal of the use of trace elements to classify and discriminate between magma series erupted in different tectonic setting. Earth and Planetary Science Letters, 1979, 45: 326~336, DOI: 10.1016/0012-821X(79)90133-X

Wang D B, Yin F G, Sun Z M, Wang L Q, Wang B D, Liao S Y, Tang Y, Ren G M. Zircon U-Pb age and Hf isotopes of Paleoproterozoic mafic intrusion on the western margin of the Yangtze Block and their implications. Geological Bulletin of China, 2013, 32(4): 617~630 (in Chinese with English abstract), DOI: 10.3969/j.issn.1671-2552.2013.04.010

Wu G Y. A preliminary discussion on the strata of Tianbaoshan Formation. Journal of Stratigraphy, 1986, 10(3): 161~168 (in Chinese with English abstract), DOI: CNKI:SUN:DCXZ.0.1986-03-000

Wang S W, Jiang X F, Yang B, Sun X M, Liao Z W, Zhou Q, Guo Y, Wang Z Z, Yang B. The Proterozoic tectonic movement in Kangdian areaI: Kunyang intracontinental rift, mantle plume and its metallogenesis. Geological Review, 2016, 62(6): 1352~1377(in Chinese with English abstract), DOI: 10.16509/j.georeview.2016.06.001

Wang W, Zhou M F. Provenance and tectonic setting of the Paleo- to Mesoproterozoic Dongchuan Group in the southwestern Yangtze Block, South China: Implication for the breakup of the supercontinent Columbia. Tectonophysics, 2014, 610: 110~127, DOI: 10.1016/j.tecto.2013.11.009

Wu Y F, Li X H, Zheng Y F, Gao L Z. Lu-Hf isotopic systematics and their applications in petrology. Acta Petrologica Sinica, 2007, 23(2): 185~220(in Chinese with English abstract), DOI: 10.1016/j.sedgeo.2006.03.028

Xu X S, Qiu J S. Igneous petrology. Beijing: Science and Technology Publishing House, 2010.

Yin F G, Sun Z M, Zhang Z. Mesoproterozoic Stratigraphic-Structure Framework in Huili-Dongchuan Area. Geological Review, 2011, 57(6): 770~778 (in Chinese with English abstract), DOI: 10.1007/s12583-011-0162-0

Yin F G, Sun Z M, Ren G M, Wang D B. Geological record of Paleo-and Mesoproterozoic

orogenesis in the western margin of upper Yangtze Block. Acta Geologica Sinica, 2012, 86(12): 1917~1932 (in Chinese with English abstract), DOI: 10.1007/s11783-011-0280-z

Yang H, Liu F L, Du L L, Liu P H, Wang F. Zircon U-Pb dating for metavolcanites in the Laochanghe Formation OF the Dahongshan Group in southwestern Yangtze Block, and it geological significance. Acta Petrologica Sinica, 2012, 28(9): 2994~3014 (in Chinese with English Abstract).

Yu S C, Tung S F, Lee J S. structural and spectroscopic features of mantle-derived zircon crystals from Tibet. Western Pacific Earth Sciences, 2001, 1(1): 47~58, DOI: http://140.127.82.166/handle/987654321/12008

Zhang C H, Liu D B, Zhang C L, Wang Z Q. Early Permian seismically induced soft-sediment deformational structures in Bogda region, Xinjiang: stratigraphic records of earthquakes in the retroarc collisional foreland basin. Earth Science Frontiers, 2006, 13(4): 255~266 (in Chinese with English abstract), DOI: 10.1007/s11442-006-0415-5

Zhang C H, Gao L Z, Wu Z J, Shi X Y, Yan Q R, Li D J. Zircon SHRIMP U-Pb age of tuff from Kunyang Group, central Yunnan Province: evidence for Granville Orogeny in south China. Chinese Science Bulletin, 2007, 52(7): 818~824 (in Chinese without English abstract), DOI: 10.1007/s11434-007-0225-x

Zhang H, Gao L Z, Zhang C H, Ding X Z, Li T D, Liu Y X. The Discovery of the 2.35Ga Crystalline Basement in the Southwest of the Yangtze Block and its Geological Significance. ACTA GEOLOGICA SINICA, 2018, 92(6): 2460~2461, DOI: CNKI:SUN:DZXW.0.2018-06-036

Zhao X F, Zhou M F, Li J W, Sun M, Gao J F, Sun W H, Yang J H. Late Paleoproterozoic to early Mesoproterozoic Dongchuan Group in Yunnan, SW China: Implications for tectonic evolution of the Yangtze Block. Precambrian Research, 2010, 182: 57~69, DOI:10.1016/j.precamres.2010.06.021

Zhao X F, Zhou M F. 2011. Fe-Cu deposits in the Kangdian region, SW China: a Proterozoic IOCG (iron-oxide-copper-gold) metallogenic province. Mineral Deposita, 2011, 46: 731~747, DOI: 10.1007/s00126-011-0342-y

Zhu W G, Zhong H, Li Z X. 2016. SIMS zircon U-Pb ages, geochemistry and Nd-Hf isotopes of ca. 1.0 Ga mafic dykes and volcanic rocks in the Huili area, SW China: Origin and Tectonic Significance. Precambrian Research, 273: 67~89, DOI: 10.1016/j.precamres.2015.12.011

Zhou M F, Zhao X F, Chen W T, Li X C, Wang W, Yan D P, Qiu H N. 2014. Proterozoic Fe–Cu metallogeny and supercontinental cycles of the southwestern Yangtze Block, southern China and northern Vietnam. Earth-Science Reviews, 139, 59–82, DOI: 10.1016/j.earscirev.2014.08.013

Table.1. Zircon U-Pb datas of A20170330-4, A20170331-1, A20170401-1 and A20170330-3

Spot	f_{206}(%)	U(ppm)	Th(ppm)	Th/U	Isotopic radio						Age/Ma		Remarks
					$^{207}Pb^*/^{206}Pb^*$	±1σ(%)	$^{207}Pb^*/^{235}U$	±1σ(%)	$^{206}Pb^*/^{238}U$	±1σ(%)	$^{207}Pb/^{206}Pb$±1σ	$^{206}Pb/^{238}U$±1σ	
A20170330-4(N27°11′32.144″, E102°15′11.014″)													
1.1	0.03	362	254	0.72	.0754	1.1	1.99	1.9	.1910	1.6	1080±21	1126.5±16.9	
2.1	-0.07	499	387	0.80	.0753	0.9	1.98	1.8	.1905	1.6	1077±18	1123.9±16.4	
3.1	-0.23	325	651	2.07	.0762	1.5	1.97	2.2	.1879	1.7	1101±30	1110.0±16.9	
4.1	-0.22	166	116	0.72	.0777	2.1	2.06	2.7	.1922	1.7	1139±41	1133.2±17.8	
~~5.1~~	~~-1.25~~	~~266~~	~~147~~	~~0.57~~	~~.0586~~	~~3.6~~	~~0.20~~	~~4.1~~	~~.0242~~	~~1.9~~	~~554±79~~	~~154.3±2.9~~	Hi 204
6.1	-0.04	757	856	1.17	.0741	0.7	1.95	1.7	.1912	1.6	1044±15	1127.9±16.3	
7.1	-0.28	131	73	0.58	.0784	2.3	2.04	2.9	.1884	1.8	1156±46	1112.7±18.0	
~~8.1~~	~~-0.09~~	~~267~~	~~209~~	~~0.81~~	~~.0997~~	~~0.9~~	~~4.14~~	~~1.9~~	~~.3011~~	~~1.6~~	~~1619±18~~	~~1696.8±24.5~~	discordant
~~9.1~~	~~-0.07~~	~~514~~	~~400~~	~~0.80~~	~~.0879~~	~~0.8~~	~~3.07~~	~~1.8~~	~~.2534~~	~~1.6~~	~~1380±15~~	~~1455.9±20.7~~	discordant
10.1	-0.09	393	239	0.63	.0749	1.1	1.97	2.0	.1912	1.6	1065±22	1128.0±16.7	
11.1	-0.06	922	1168	1.31	.0762	0.7	2.01	1.7	.1908	1.6	1100±14	1126.0±16.3	
12.1	-0.14	261	179	0.71	.0781	1.2	2.05	2.2	.1901	1.9	1148±24	1121.7±19.4	
~~13.1~~	~~-0.07~~	~~176~~	~~126~~	~~0.74~~	~~.0979~~	~~1.1~~	~~3.96~~	~~2.0~~	~~.2933~~	~~1.7~~	~~1584±20~~	~~1657.9±24.8~~	discordant
~~14.1~~	~~-0.14~~	~~146~~	~~25~~	~~0.18~~	~~.0779~~	~~1.6~~	~~2.15~~	~~2.6~~	~~.2001~~	~~2.1~~	~~1145±31~~	~~1176.0±22.3~~	
~~15.1~~	~~-0.07~~	~~357~~	~~105~~	~~0.30~~	~~.0892~~	~~0.9~~	~~3.20~~	~~1.8~~	~~.2601~~	~~1.6~~	~~1409±16~~	~~1490.2±21.5~~	discordant
16.1	-0.11	267	90	0.35	.0766	1.4	2.05	2.1	.1938	1.6	1111±27	1141.7±17.2	
17.1	-0.03	368	378	1.06	.0761	1.0	2.02	2.0	.1926	1.7	1098±20	1135.4±17.7	
18.1	-0.10	240	30	0.13	.0742	1.8	1.96	2.4	.1910	1.7	1048±36	1127.0±17.1	
A20170331-1(N27°11′31.081″, E102°15′10.721″)													
1.1	-0.09	176	1650	9.66	.0743	1.8	1.86	2.5	.1812	1.7	1050±35	1073.3±16.9	
2.1	-0.03	330	57	0.18	.0745	1.2	1.94	2.0	.1890	1.6	1056±23	1115.8±16.7	
3.1	-0.03	203	58	0.29	.0743	1.5	1.86	2.3	.1813	1.7	1048±30	1074.1±16.7	
4.1	-0.09	294	435	1.53	.0763	1.3	1.98	2.1	.1880	1.6	1103±27	1110.5±16.8	
~~5.1~~	~~0.07~~	~~550~~	~~183~~	~~0.34~~	~~.0723~~	~~1.6~~	~~1.73~~	~~2.2~~	~~.1734~~	~~1.6~~	~~994±32~~	~~1030.7±15.2~~	Hi U

Spot	f_{206}(%)	U(ppm)	Th(ppm)	Th/U	Isotopic radio						Age/Ma		Remarks
					$^{207}Pb^*/^{206}Pb^*$	±1σ(%)	$^{207}Pb^*/^{235}U$	±1σ(%)	$^{206}Pb^*/^{238}U$	±1σ(%)	$^{207}Pb/^{206}Pb$±1σ	$^{206}Pb/^{238}U$±1σ	
~~6.1~~	~~0.07~~	~~336~~	~~79~~	~~0.24~~	~~.0735~~	~~1.3~~	~~1.76~~	~~2.2~~	~~.1736~~	~~1.7~~	~~1029±26~~	~~1032.0±16.5~~	Hi 204
7.1	-0.06	170	66	0.40	.0781	1.6	2.03	2.6	.1886	2.0	1150±31	1113.7±20.7	
8.1	-0.06	527	553	1.09	.0742	1.0	1.91	1.9	.1866	1.6	1046±20	1102.8±16.2	
9.1	-0.08	218	46	0.22	.0755	1.6	1.98	2.3	.1904	1.7	1082±32	1123.6±17.3	
~~10.1~~	~~1.70~~	~~703~~	~~158~~	~~0.23~~	~~.0723~~	~~0.8~~	~~1.77~~	~~1.8~~	~~.1773~~	~~1.6~~	~~994±16~~	~~1052.2±15.3~~	Hi U
~~11.1~~	~~0.01~~	~~145~~	~~149~~	~~1.06~~	~~.0983~~	~~1.2~~	~~3.86~~	~~2.1~~	~~.2847~~	~~1.7~~	~~1591±23~~	~~1614.8±24.8~~	Hi 204
12.1	-0.04	258	194	0.78	.0752	1.2	1.95	2.1	.1880	1.7	1075±25	1110.8±16.9	
~~13.1~~	~~-0.13~~	~~217~~	~~72~~	~~0.34~~	~~.0746~~	~~1.7~~	~~1.83~~	~~2.4~~	~~.1780~~	~~1.7~~	~~1057±34~~	~~1056.0±16.4~~	Hi U
14.1	-0.44	177	52	0.30	.0763	2.3	2.02	3.4	.1919	2.6	1104±45	1131.6±26.8	
15.1	-0.05	201	51	0.26	.0747	1.5	1.86	2.3	.1806	1.7	1062±31	1070.3±16.7	
A20170401-1(N26°28′35.46″, E102°5′33.115″)													
1.1	0.03	586	50	0.09	0.07208	0.85	1.766	1.9	0.1777	1.7	988±17	1054.4±16.6	
~~2.1~~	~~0.07~~	~~256~~	~~107~~	~~0.43~~	~~0.08507~~	~~1.1~~	~~2.638~~	~~2.1~~	~~0.2249~~	~~1.8~~	~~1317±20~~	~~1307.8±21.0~~	~~Hi Th/U~~
~~3.1~~	~~0.24~~	~~2488~~	~~7181~~	~~2.98~~	~~0.06600~~	~~0.97~~	~~0.955~~	~~1.9~~	~~0.1050~~	~~1.7~~	~~806±20~~	~~643.4±10.3~~	~~Hi U~~
~~4.1~~	~~0.14~~	~~168~~	~~125~~	~~0.77~~	~~0.0960~~	~~1.3~~	~~3.602~~	~~2.2~~	~~0.2722~~	~~1.8~~	~~1547±24~~	~~1552.2±25.2~~	~~Hi Th/U~~
5.1	0.10	213	31	0.15	0.0753	1.8	1.791	3.1	0.1725	2.4	1077±37	1025.6±23.1	
6.1	0.08	342	56	0.17	0.0754	1.4	1.853	2.2	0.1783	1.8	1078±27	1057.5±17.3	
7.1	0.13	2004	4699	2.42	0.07167	0.61	1.665	1.8	0.1685	1.7	977±13	1004.0±15.6	
~~8.1~~	~~0.43~~	~~543~~	~~98~~	~~0.19~~	~~0.08436~~	~~1.1~~	~~2.201~~	~~2.0~~	~~0.1892~~	~~1.7~~	~~1301±22~~	~~1117.2±17.6~~	~~Hi 204~~
~~9.1~~	~~0.17~~	~~338~~	~~40~~	~~0.12~~	~~0.08409~~	~~1.2~~	~~2.383~~	~~2.1~~	~~0.2055~~	~~1.8~~	~~1295±23~~	~~1205.0±19.5~~	~~discordant~~
10.1	0.30	199	24	0.12	0.0756	2.3	1.798	2.9	0.1724	1.8	1085±46	1025.6±17.3	
11.1	--	145	83	0.59	0.0771	1.7	1.848	2.9	0.1739	2.4	1123±33	1033.6±23.1	
~~12.1~~	~~0.34~~	~~162~~	~~127~~	~~0.80~~	~~0.1653~~	~~0.86~~	~~10.39~~	~~2.3~~	~~0.4559~~	~~2.2~~	~~2511±14~~	~~2421.5±44.0~~	~~Hi 204~~
A20170330-3(N27°11′35.957″, E102°15′11.239″)													
1.1	-0.24	242	83	0.35	.0736	1.8	1.77	2.5	.1745	1.7	1030±37	1036.9±16.4	
2.1	-0.33	143	54	0.39	.0738	2.5	1.80	3.1	.1775	1.8	1035±51	1053.2±17.2	

Spot	f_{206}(%)	U(ppm)	Th(ppm)	Th/U	Isotopic radio						Age/Ma		Remarks
					$^{207}Pb^*/^{206}Pb^*$	±1σ(%)	$^{207}Pb^*/^{235}U$	±1σ(%)	$^{206}Pb^*/^{238}U$	±1σ(%)	$^{207}Pb/^{206}Pb$±1σ	$^{206}Pb/^{238}U$±1σ	
3.1	0.00	128	47	0.38	.0769	1.9	1.92	2.6	.1806	1.8	1119±38	1070.3±17.7	
4.1	-0.21	230	88	0.39	.0741	3.1	1.86	3.5	.1818	1.7	1044±63	1076.7±16.8	
5.1	-0.16	168	59	0.36	.0753	2.0	1.85	3.2	.1783	2.5	1076±41	1057.5±24.1	
~~6.1~~	~~0.00~~	~~724~~	~~378~~	~~0.54~~	~~.0729~~	~~0.8~~	~~1.89~~	~~1.8~~	~~.1880~~	~~1.6~~	~~1012±16~~	~~1110.5±16.1~~	Hi U
7.1	-0.10	503	134	0.28	.0741	1.1	1.81	1.9	.1770	1.6	1044±22	1050.4±15.5	
8.1	-0.18	321	111	0.36	.0741	1.5	1.84	2.2	.1798	1.6	1043±31	1065.7±16.1	
9.1	-0.25	190	76	0.42	.0761	1.8	1.84	2.5	.1755	1.7	1097±36	1042.4±16.5	
10.1	0.06	208	134	0.67	.0736	1.6	1.72	2.3	.1695	1.7	1030±32	1009.3±15.8	Hi Th/U
11.1	0.07	284	97	0.35	.0742	1.3	1.76	2.1	.1723	1.6	1047±26	1024.7±15.6	
12.1	-0.18	221	117	0.55	.0739	1.4	1.86	2.2	.1821	1.7	1038±28	1078.3±16.7	
13.1	0.00	266	98	0.38	.0741	1.3	1.76	2.1	.1724	1.7	1045±26	1025.4±15.9	
14.1	1.07	371	99	0.28	.0734	2.4	1.83	2.9	.1808	1.6	1024±49	1071.5±16.2	
15.1	-0.19	278	72	0.27	.0729	1.6	1.80	2.3	.1791	1.6	1012±33	1062.1±16.1	

Table.2. Zircon U-Pb datas of A20170414-1

Spot	concordance	U(ppm)	Th(ppm)	Isotopic radio						Age/Ma		Remarks
				$^{207}Pb^*/^{206}Pb^*$	±1σ(%)	$^{207}Pb^*/^{235}U$	±1σ(%)	$^{206}Pb^*/^{238}U$	±1σ(%)	$^{207}Pb/^{206}Pb$±1σ	$^{206}Pb/^{238}U$±1σ	
A20170414-1(N27°11′24.684″, E102°15′9.107″)												
01	94%	830	316	0.0976	0.0023	3.2963	0.0742	0.2426	0.0020	1589±44	1400±10	Higher LREE
02	95%	199	118	0.1159	0.0027	4.9447	0.1089	0.3072	0.0024	1894±42	1727±12	
03	97%	167	141	0.1066	0.0025	4.2946	0.0979	0.2903	0.0024	1743±43	1643±12	
04	94%	444	149	0.1059	0.0071	4.6766	0.4194	0.2966	0.0046	1729±76	1675±23	CorComPb
05	94%	331	88.1	0.1388	0.0029	6.9452	0.1442	0.3607	0.0027	2213±37	1985±13	
06	91%	382	101	0.1318	0.0030	5.8152	0.1334	0.3185	0.0029	2124±39	1783±14	
07	97%	255	153	0.1472	0.0033	8.2845	0.1829	0.4060	0.0030	2314±37	2196±14	
08	98%	359	253	0.0890	0.0051	3.1460	0.2262	0.2458	0.0027	1406±105	1417±14	CorComPb
09	94%	609	662	0.1009	0.0022	3.5549	0.0802	0.2532	0.0017	1643±159	1455±9	
10	90%	162	144	0.1183	0.0037	4.5298	0.1265	0.2772	0.0026	1931±56	1577±13	Higher LREE
11	98%	479	244	0.0969	0.0022	3.6311	0.0884	0.2686	0.0029	1566±42	1534±15	
12	98%	312	105	0.1066	0.0025	4.5286	0.1042	0.3049	0.0025	1742±44	1715±13	
13	96%	372	872	0.0875	0.0022	2.6542	0.0638	0.2177	0.0017	1372±49	1270±9	
14	94%	654	631	0.0847	0.0033	2.3228	0.0923	0.1967	0.0017	1309±76	1158±9	
15	99%	398	291	0.0796	0.0019	2.2358	0.0524	0.2014	0.0016	1188±46	1183±9	
16	97%	202	245	0.1008	0.0024	3.8604	0.0870	0.2754	0.0023	1639±44	1568±11	
17	97%	221	74.1	0.1090	0.0024	4.5875	0.0972	0.3025	0.0022	1783±40	1704±11	
18	96%	187	163	0.1139	0.0025	4.9898	0.1057	0.3146	0.0023	1865±34	1763±11	
19	91%	390	150	0.1261	0.0027	5.4119	0.1113	0.3085	0.0026	2056±38	1733±13	
20	98%	396	99.1	0.1131	0.0024	5.1351	0.1056	0.3262	0.0024	1850±37	1820±12	
21	95%	358	209	0.1190	0.0028	5.2508	0.1186	0.3186	0.0036	1943±42	1783±18	
22	98%	193	203	0.1074	0.0026	4.5895	0.1054	0.3076	0.0025	1767±38	1729±12	
23	98%	237	355	0.0924	0.0024	3.2186	0.0825	0.2507	0.0022	1476±50	1442±11	
24	98%	134	120	0.0975	0.0029	3.6383	0.1028	0.2687	0.0025	1577±55	1534±13	

Spot	concordance	U(ppm)	Th(ppm)	Isotopic radio						Age/Ma		Remarks
				$^{207}Pb^*/^{206}Pb^*$	±1σ(%)	$^{207}Pb^*/^{235}U$	±1σ(%)	$^{206}Pb^*/^{238}U$	±1σ(%)	$^{207}Pb/^{206}Pb$±1σ	$^{206}Pb/^{238}U$±1σ	
25	95%	358	62.4	0.0995	0.0022	3.4884	0.0773	0.2523	0.0020	1615±43	1450±10	
26	96%	282	233	0.1055	0.0025	4.0888	0.0934	0.2792	0.0021	1724±43	1587±10	
27	97%	410	189	0.1086	0.0021	4.5556	0.0880	0.3017	0.0021	1776±37	1700±10	
28	99%	488	61.8	0.0919	0.0019	3.2754	0.0680	0.2562	0.0022	1466±39	1470±11	
29	98%	497	318	0.0937	0.0021	3.3545	0.0794	0.2572	0.0022	1502±43	1475±11	
30	96%	364	813	0.1581	0.0037	9.4902	0.2213	0.4315	0.0037	2435±40	2313±17	
31	92%	605	409	0.1053	0.0026	3.7516	0.0917	0.2562	0.0021	1720±46	1470±11	
32	96%	118	68.1	0.0935	0.0023	3.1565	0.0767	0.2430	0.0021	1498±46	1402±11	
33	96%	417	245	0.0919	0.0019	2.9963	0.0616	0.2351	0.0020	1465±36	1361±10	Higher LREE
34	93%	484	369	0.0957	0.0020	3.0634	0.0643	0.2303	0.0018	1543±40	1336±9	
35	95%	245	195	0.0947	0.0022	3.1693	0.0758	0.2410	0.0021	1521±45	1392±11	CorComPb
36	94%	474	637	0.1651	0.0037	9.6645	0.2204	0.4213	0.0040	2509±38	2266±18	
37	92%	409	62.0	0.1311	0.0033	6.0348	0.1539	0.3310	0.0029	2113±49	1843±14	Tresis
38	94%	222	98.0	0.0961	0.0022	3.1243	0.0754	0.2342	0.0023	1550±43	1356±12	
39	90%	363	203	0.1080	0.0024	3.8687	0.1454	0.2537	0.0067	1766±40	1457±34	
40	98%	310	188	0.1388	0.0028	7.6333	0.1527	0.3960	0.0027	2213±35	2151±12	
41	93%	294	114	0.1190	0.0027	5.0474	0.1127	0.3054	0.0024	1943±40	1718±12	
42	97%	379	328	0.1010	0.0025	3.8922	0.0939	0.2777	0.0024	1643±46	1580±12	
43	98%	137	70.5	0.1097	0.0030	4.7997	0.1282	0.3151	0.0027	1794±49	1766±13	
44	96%	767	310	0.0870	0.0020	2.6048	0.0593	0.2156	0.0019	1361±43	1258±10	
45	98%	373	116	0.1140	0.0023	5.1489	0.1004	0.3249	0.0024	1865±37	1814±12	
46	99%	287	109	0.1035	0.0021	4.3259	0.0896	0.3007	0.0028	1688±38	1695±14	
47	97%	317	121	0.1077	0.0022	4.4211	0.0891	0.2949	0.0022	1761±38	1666±11	
48	97%	298	203	0.1058	0.0024	4.2591	0.0898	0.2894	0.0023	1728±41	1638±12	
49	90%	329	236	0.1319	0.0029	5.7443	0.1259	0.3129	0.0030	2124±39	1755±15	
50	95%	194	210	0.1062	0.0025	4.1520	0.1019	0.2805	0.0027	1800±43	1594±14	

Spot	concordance	U(ppm)	Th(ppm)	Isotopic radio						Age/Ma		Remarks
				$^{207}Pb^*/^{206}Pb^*$	±1σ(%)	$^{207}Pb^*/^{235}U$	±1σ(%)	$^{206}Pb^*/^{238}U$	±1σ(%)	$^{207}Pb/^{206}Pb$±1σ	$^{206}Pb/^{238}U$±1σ	
51	96%	226	111	0.1101	0.0024	4.5308	0.1020	0.2959	0.0029	1811±40	1671±15	
52	96%	445	203	0.0916	0.0018	3.5533	0.0685	0.2790	0.0025	1461±31	1587±12	
53	98%	472	249	0.1090	0.0020	4.6665	0.0835	0.3084	0.0023	1783±34	1733±11	
54	99%	404	81.3	0.0888	0.0017	3.0249	0.0584	0.2451	0.0019	1400±36	1413±10	

Table.3. Zircon Lu-Hf isotopes datas of A20170330-4 and A20170331-1

Spot	t(Ma)	$^{176}Yb/^{177}Hf$	$^{176}Lu/^{177}Hf$	$^{176}Hf/^{177}Hf$	2σ	$(^{176}Hf/^{177}Hf)_i$	$\varepsilon_{Hf}(t)$	2σ	T_{DM}(Ma)	T^C_{DM}(Ma)	$f_{Lu/Hf}$
A20170330-4(N27°11′32.144″, E102°15′11.014″)											
1.1	1126.5	0.09	0.001998	0.282265	0.000022	0.282223	5.5	0.8	1432	1610	-0.94
2.1	1123.9	0.06	0.001307	0.282299	0.000019	0.282271	7.2	0.7	1357	1501	-0.96
~~3.1~~	~~1110.0~~	~~0.11~~	~~0.002430~~	~~0.282397~~	~~0.000032~~	~~0.282346~~	~~9.5~~	~~1.1~~	~~1257~~	~~1340~~	~~-0.93~~
~~4.1~~	~~1133.2~~	~~0.13~~	~~0.002787~~	~~0.282354~~	~~0.000027~~	~~0.282294~~	~~8.2~~	~~1.0~~	~~1332~~	~~1442~~	~~-0.92~~
~~5.1~~	~~154.3~~	~~0.05~~	~~0.001109~~	~~0.282526~~	~~0.000022~~	~~0.282523~~	~~-5.4~~	~~0.8~~	~~1031~~	~~1549~~	~~-0.97~~
~~6.1~~	~~1127.9~~	~~0.12~~	~~0.002667~~	~~0.282355~~	~~0.000022~~	~~0.282298~~	~~8.2~~	~~0.8~~	~~1326~~	~~1437~~	~~-0.92~~
7.1	1112.7	0.04	0.000835	0.282314	0.000017	0.282296	7.8	0.6	1320	1451	-0.97
~~8.1~~	~~1696.8~~	~~0.04~~	~~0.001099~~	~~0.281929~~	~~0.000016~~	~~0.281894~~	~~6.7~~	~~0.6~~	~~1866~~	~~1975~~	~~-0.97~~
~~9.1~~	~~1455.9~~	~~0.06~~	~~0.001287~~	~~0.282041~~	~~0.000021~~	~~0.282006~~	~~5.2~~	~~0.7~~	~~1719~~	~~1884~~	~~-0.96~~
~~10.1~~	~~1128.0~~	~~0.13~~	~~0.002701~~	~~0.282345~~	~~0.000022~~	~~0.282288~~	~~7.8~~	~~0.8~~	~~1342~~	~~1462~~	~~-0.92~~
~~11.1~~	~~1126.0~~	~~0.14~~	~~0.002964~~	~~0.282375~~	~~0.000021~~	~~0.282312~~	~~8.7~~	~~0.7~~	~~1308~~	~~1407~~	~~-0.91~~
12.1	1121.7	0.07	0.001509	0.282254	0.000022	0.282222	5.4	0.8	1428	1615	-0.95
~~13.1~~	~~1657.9~~	~~0.04~~	~~0.001098~~	~~0.281986~~	~~0.000017~~	~~0.281952~~	~~7.9~~	~~0.6~~	~~1787~~	~~1870~~	~~-0.97~~
~~14.1~~	~~1176.0~~	~~0.05~~	~~0.001087~~	~~0.282173~~	~~0.000016~~	~~0.282149~~	~~4.0~~	~~0.6~~	~~1526~~	~~1745~~	~~-0.97~~
~~15.1~~	~~1490.2~~	~~0.05~~	~~0.001238~~	~~0.281922~~	~~0.000020~~	~~0.281887~~	~~1.8~~	~~0.7~~	~~1883~~	~~2130~~	~~-0.96~~
16.1	1141.7	0.07	0.001584	0.282069	0.000017	0.282035	-0.8	0.6	1693	2025	-0.95
~~17.1~~	~~1135.4~~	~~0.20~~	~~0.003984~~	~~0.282447~~	~~0.000029~~	~~0.282362~~	~~10.6~~	~~1.0~~	~~1237~~	~~1287~~	~~-0.88~~
18.1	1127.0	0.01	0.000165	0.282076	0.000015	0.282072	0.2	0.5	1622	1950	-1.00

Spot	t(Ma)	$^{176}Yb/^{177}Hf$	$^{176}Lu/^{177}Hf$	$^{176}Hf/^{177}Hf$	2σ	$(^{176}Hf/^{177}Hf)_i$	$\varepsilon_{Hf}(t)$	2σ	T_{DM}(Ma)	T^{C}_{DM}(Ma)	$f_{Lu/Hf}$
A20170331-1(N27°11′31.081″, E102°15′10.721″)											
1.1	1073.3	0.04	0.000865	0.282426	0.000016	0.282409	10.9	0.6	1164	1222	-0.97
2.1	1115.8	0.02	0.000425	0.282153	0.000015	0.282144	2.5	0.5	1527	1795	-0.99
3.1	1074.1	0.05	0.001164	0.281929	0.000017	0.281905	-6.9	0.6	1869	2359	-0.96
4.1	1110.5	0.09	0.002011	0.282285	0.000016	0.282243	5.9	0.6	1403	1575	-0.94
~~5.1~~	~~1030.7~~	~~0.04~~	~~0.000901~~	~~0.281980~~	~~0.000017~~	~~0.281963~~	~~-5.9~~	~~0.6~~	~~1786~~	~~2259~~	~~-0.97~~
~~6.1~~	~~1032.0~~	~~0.04~~	~~0.000835~~	~~0.281944~~	~~0.000015~~	~~0.281928~~	~~-7.1~~	~~0.5~~	~~1832~~	~~2336~~	~~-0.97~~
7.1	1113.7	0.03	0.000764	0.282207	0.000018	0.282191	4.1	0.6	1466	1691	-0.98
8.1	1102.8	0.05	0.001146	0.282186	0.000017	0.282162	2.8	0.6	1510	1763	-0.97
9.1	1123.6	0.03	0.000639	0.282132	0.000015	0.282118	1.8	0.5	1564	1848	-0.98
~~10.1~~	~~1052.2~~	~~0.07~~	~~0.001589~~	~~0.282007~~	~~0.000016~~	~~0.281976~~	~~-4.9~~	~~0.6~~	~~1781~~	~~2216~~	~~-0.95~~
~~11.1~~	~~1614.8~~	~~0.11~~	~~0.002524~~	~~0.282109~~	~~0.000022~~	~~0.282032~~	~~9.8~~	~~0.8~~	~~1679~~	~~1716~~	~~-0.92~~
12.1	1110.8	0.09	0.002023	0.282064	0.000025	0.282022	-2.0	0.9	1720	2075	-0.94
~~13.1~~	~~1056.0~~	~~0.04~~	~~0.000883~~	~~0.282026~~	~~0.000016~~	~~0.282008~~	~~-3.7~~	~~0.6~~	~~1721~~	~~2140~~	~~-0.97~~
14.1	1131.6	0.05	0.001172	0.282001	0.000016	0.281976	-3.1	0.6	1769	2164	-0.96
15.1	1070.3	0.05	0.001131	0.282029	0.000017	0.282006	-3.4	0.6	1729	2136	-0.97

Table.4. Geochemistrical datas

Items \ Numbers	SiO2（%）	Al_2O_3（%）	TiO_2（%）	Fe_2O_3（%）	FeO（%）	CaO（%）	MgO（%）	K_2O（%）	Na_2O（%）	MnO（%）	P_2O_5（%）	H_2O^+（%）	H_2O^-（%）	Loss on ignition（%）	Y（μg/g）	La（μg/g）
C20170330-1	46.96	15.71	2.09	1.94	10.79	10.26	6.23	0.69	2.66	0.24	0.21	1.23	0.15	2.07	31.3	11.2
C20170330-2	46.76	15.13	2.18	2.07	11.59	10.37	6.26	0.48	2.71	0.23	0.22	0.91	0.11	1.84	35	13.2
C20170330-3	48.47	15.97	1.5	1.99	10.26	9.95	5.93	0.5	3.12	0.23	0.16	0.86	0.12	1.8	37.1	14.2
C20170330-5	46.42	15.2	2.04	2.03	10.74	10.32	6.94	0.75	2.01	0.22	0.24	2.38	0.29	2.97	35.6	14.9
C20170330-9	46.54	15.97	2.03	2.5	9.93	10.89	5.93	0.67	2.62	0.22	0.2	1.66	0.21	2.37	28.8	14.7
Items \ Numbers	Ce（μg/g）	Pr（μg/g）	Nd（μg/g）	Sm（μg/g）	Eu（μg/g）	Gd（μg/g）	Tb（μg/g）	Dy（μg/g）	Ho（μg/g）	Er（μg/g）	Tm（μg/g）	Yb（μg/g）	Lu（μg/g）	Li（μg/g）	Be（μg/g）	Sc（μg/g）

C20170330-1	22.9	3.33	15.7	4.41	1.7	4.43	0.92	5.9	1.13	3.16	0.55	3.29	0.52	8.08	0.71	38.2
C20170330-2	26.6	3.87	18.2	5.03	1.69	5.03	1.04	6.7	1.29	3.56	0.62	3.62	0.58	6.06	0.77	39.5
C20170330-3	30.7	4.63	21.6	5.84	1.79	5.74	1.17	7.41	1.42	3.9	0.68	4.02	0.62	8.91	1.05	26.6
C20170330-5	31.4	4.58	20.9	5.28	1.96	5.26	1.08	6.72	1.31	3.65	0.63	3.8	0.61	18.5	0.82	34.4
C20170330-9	30.8	4.1	18	4.48	1.69	4.48	0.89	5.59	1.07	2.97	0.51	3.03	0.49	15.3	0.77	48.4

Items \ Numbers	V（μg/g）	Cr（μg/g）	Co（μg/g）	Ni（μg/g）	Cu（μg/g）	Zn（μg/g）	Ga（μg/g）	Ge（μg/g）	Rb（μg/g）	Sr（μg/g）	Zr（μg/g）	Nb（μg/g）	Mo（μg/g）	Cd（μg/g）	In（μg/g）	Sn（μg/g）
C20170330-1	302	190	62	49.9	36.8	157	21.6	1.64	29.3	234	96.7	10.4	0.35	0.24	0.12	2.49
C20170330-2	322	212	69.2	54.9	31.1	159	23	1.72	14.3	226	124	12.5	0.24	0.12	0.12	1.62
C20170330-3	223	111	51.1	50.2	12.9	137	22.1	1.58	23.5	252	176	12.7	0.4	0.17	0.14	2.15
C20170330-5	231	147	55.6	38.3	30	133	21.8	1.7	80	249	129	8.7	0.73	0.2	0.098	1.16
C20170330-9	279	169	50.9	46.9	14.4	140	22.2	1.71	48.8	245	97.6	10.3	0.13	0.19	0.12	2.96

Items \ Numbers	Cs（μg/g）	Ba（μg/g）	Hf（μg/g）	Ta（μg/g）	W（μg/g）	Tl（μg/g）	Pb（μg/g）	Bi（μg/g）	Th（μg/g）	U（μg/g）	ΣREE	LREE	HREE	LREE/HREE	La_N/Yb_N	δEu
C20170330-1	1.34	182	3.02	0.6	0.47	0.15	9	0.098	1.85	0.3	79.14	59.24	19.91	2.96	3.21	1.25
C20170330-2	0.63	157	3.81	0.77	0.41	0.083	3.98	0.051	1.66	0.36	91.06	68.63	22.43	3.06	3.43	1.09
C20170330-3	0.73	145	5.65	1.07	0.75	0.23	4.99	0.055	7.81	0.5	103.67	78.71	24.96	3.15	3.32	1.01
C20170330-5	24.9	131	3.76	0.5	0.26	0.9	2.95	0.025	0.92	0.23	102.06	79.01	23.05	3.43	3.70	1.21
C20170330-9	2.23	263	3.24	0.66	1.06	0.25	5.3	0.15	1.56	0.52	92.83	73.81	19.03	3.88	4.59	1.22